

Room temperature synthesis of UO_{2+x} nanocrystals and thin films via hydrolysis of uranium(IV) complexes

Journal:	<i>Inorganic Chemistry Frontiers</i>
Manuscript ID	QI-RES-09-2021-001248.R1
Article Type:	Research Article
Date Submitted by the Author:	09-Nov-2021
Complete List of Authors:	<p>Murillo, Jesse; University of Texas at El Paso, Chemistry Panda, Debiprasad; Indian Institute of Technology Bombay Chakrabarti, Subhananda; Indian Institute of Technology Bombay, Electrical Hattori, Alex; University of Texas at El Paso, Department of Chemistry and Biochemistry Griego, Leonel; University of Texas at El Paso, Department of Chemistry and Biochemistry Chava, Venkata Surya N; University of Texas at El Paso, Chemistry and Biochemistry Sreenivasan, Sreeprasad; The University of Texas at El Paso, Chemistry and Biochemistry Ramana, Chintalapalle; University of Texas at El Paso, Mechanical Engineering Fortier, Skye; University of Texas at El Paso, Department of Chemistry</p>

ARTICLE

Room temperature synthesis of UO_{2+x} nanocrystals and thin films via hydrolysis of uranium(IV) complexes

Received 00th January 20xx,
Accepted 00th January 20xx

Jesse Murillo,^a Debiprasad Panda,^b Subhananda Chakrabarti,^b Alex Hattori,^a Leonel Griego,^a Venkata S. N. Chava,^a Sreeprasad T. Sreenivasan,^a C. V. Ramana,^{c,d} and Skye Fortier^{*a}

DOI: 10.1039/x0xx00000x

Methods for the straightforward, room temperature synthesis of UO_{2+x} nanoparticles and thin films using solution processable, molecular uranium(IV) compounds is described. Ultra-small uranium dioxide nanoparticles are synthesized from the hydrolysis of either $\text{U}(\text{ditox})_4$ (ditox = $^-\text{OCH}^t\text{Bu}_2$) (**1**) or $\text{U}(\text{CH}_2\text{SiMe}_2\text{NSiMe}_3)[\text{N}(\text{SiMe}_3)_2]_2$ (**2**) via addition of water to stirring solutions of the compounds in non-polar solvents to give UO_2 -**1** and UO_2 -**2**, respectively. The structural characteristics of the uranium dioxide nanoparticles were characterized using powder X-ray diffraction (pXRD), high-resolution transmission electron microscopy (HRTEM), and Raman spectroscopy. The pXRD results affirm the cubic fluorite structure expected for UO_2 nanoparticles. The nanocrystallinity of UO_2 -**1** and UO_2 -**2** were substantiated by bright-field HRTEM images and fast Fourier transform (FFT) patterns. The HRTEM analysis also shows the nanoparticles fall within the ultra-small regime possessing sizes of ~ 3 nm with uniform distribution. Additionally, we demonstrate the versatility of **1** as a uranium dioxide precursor, showing that it can be readily sublimed onto glass or silicon substrates and subsequently hydrolyzed to give UO_{2+x} thin films.

Introduction

The physical properties of uranium oxides have been extensively studied due to their various roles in the nuclear fuel cycle. In particular, UO_2 has received much attention as this binary oxide is utilized as the primary fuel source in nuclear reactors. The study of UO_2 has revealed this material to have a number of interesting properties that could be utilized in a wide range of applications. For instance, UO_2 has been demonstrated to be capable of performing the heterogeneous catalytic hydrodesulphurization of H_2S and the dehydrogenation of ethyl benzene and ethanol.¹⁻³ UO_2 can also be readily oxidized to U_3O_8 , which has been used in the oxidation of volatile organic compounds.⁴

Moreover, UO_2 single crystals possess a high Seebeck coefficient of ca. 750 $\mu\text{V}/\text{K}$ that signals possible use for thermoelectric applications, though this can vary in polycrystalline samples based on grain size.⁵ UO_2 also has interesting semiconducting properties that vary upon the relative oxygen content. Technically, it is a Mott-Hubbard insulator^{6,7} with a band gap of ca. 2.0 eV⁸⁻¹⁰ that can range from

0.54 eV in $\text{UO}_{1.97}$ to 1.68 eV in $\text{UO}_{2.25}$ based on hypo- or hyperstoichiometric oxygen content, respectively.^{9, 11, 12} As proof of principle of its semiconducting character, UO_2 has been used to construct a Schottky diode¹³ and has also been used in gas sensing devices.¹⁴ The conductivity of UO_2 increases with higher temperatures,^{15, 16} providing an advantage over traditional semiconducting materials such as Si or GaAs.

A complicating factor in the use of UO_2 is its high melting point, 2805 $^\circ\text{C}$,¹⁷ which can potentially limit its applications. Sputtering has traditionally been used for fabricating thin films,¹⁸ while sol-gel methods,^{14, 19-21} hydrothermal syntheses,^{4, 22-27} gamma ray or electron beam irradiation,²⁸⁻³⁰ and galvanostatic reduction of uranyl^{31,32} have been used for the synthesis of UO_2 nanoparticles. Sol-gel methods and hydrothermal syntheses are the most practical because these techniques generally involve straightforward preparations. These routes typically rely on the reductive, thermal decomposition of uranyl(VI) in gelled organic matrices to UO_2 , which may lead to the incorporation of carbon impurities or the undesired formation of mixed valent binary oxides. The use of uranium(IV) oxalate has been reported in the hydrothermal synthesis of UO_2 .^{24,25} In principle, this avoids the adventitious formation of mixed valent oxides, though high temperatures and pressures are still required.

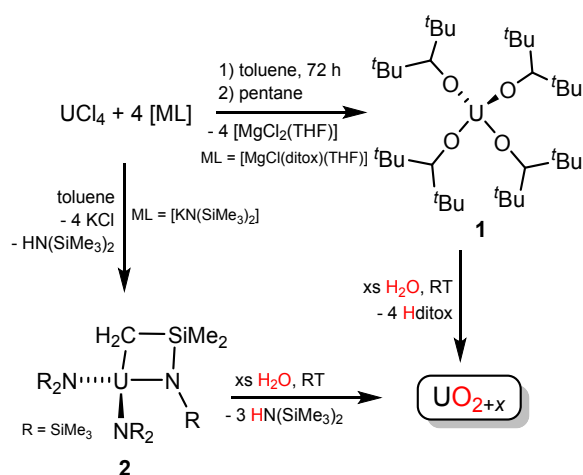
Exciting progress in the chemical vapor deposition (CVD) of uranium oxides using volatile uranium(IV) compounds has been reported.³³⁻³⁵ In 2014, Mathur, Evans, and co-workers described the gas phase conversion of air-stable uranium(IV) β -heteroarylalkenolates to form UO_3 and U_3O_8 films using CVD.³³ Later, Mathur et al. demonstrated that volatile uranium(IV)

^aDepartment of Chemistry and Biochemistry, University of Texas at El Paso, El Paso, Texas 79968, United States.

^bCentre for Nanoelectronics, Department of Electrical Engineering, Indian Institute of Technology Bombay, Mumbai 400076, India.

^cCenter for Advanced Materials Research (CMR), University of Texas at El Paso, El Paso, Texas 79968, United States. ^dDepartment of Mechanical Engineering, University of Texas at El Paso, El Paso, Texas 79968, United States.

Electronic Supplementary Information (ESI) available: Crystallographic details, spectra, and profilometry data. See DOI: 10.1039/x0xx00000x



Scheme 1. Synthesis of **1** and **2** and hydrolysis to UO_2 .

amidinate complexes could be used for the CVD of phase-pure UO_2 thin films. More recently, the uranium(VI) alkoxide complex $\text{U}(\text{O}^t\text{Bu})_6$ was shown to undergo reductive decomposition through CVD to give UO_2 films.³⁵ Interestingly, application of a magnetic field during the process alters the morphology and orientation of the films.

In our own laboratory, we have been exploring chemically well-defined uranium(IV) molecular precursors that could be used for the synthesis of both UO_2 nanoparticles and thin films. Special consideration has been given to complexes that are soluble in a wide range of organic solvents for improved processability, sublimable under moderate conditions, and that instantaneously hydrolyse to UO_2 upon exposure to water. Based upon this criteria, we have focused our attention on two previously reported molecules developed by the Andersen laboratory, namely $\text{U}(\text{ditox})_4$ (ditox = $^-\text{OCH}^t\text{Bu}_2$) (**1**)^{36, 37} and the metallacycle $\text{U}(\text{CH}_2\text{SiMe}_2\text{NSiMe}_3)[\text{N}(\text{SiMe}_3)_2]_2$ (**2**).³⁸

Compounds **1** and **2** have long been known but are repurposed here for new applications in actinide materials science. We describe the modified synthesis and structural characterization of **1** and its use in the synthesis of UO_{2+x} nanocrystals. We additionally detail use of **2** for this purpose. The resulting uranium dioxide nanocrystalline powders have been characterised by powder X-ray diffraction (pXRD), FT-IR and Raman spectroscopies, and high-resolution transmission electron microscopy (HRTEM). Furthermore, we demonstrate the viability of **1** for preparing thin films of UO_{2+x} . The use of **1** and **2** provides easy entry to the synthesis of UO_{2+x} nanoparticles and thin films under mild conditions with common laboratory equipment.

Results and discussion

Synthesis of UO_2 nanoparticles

Compound **1** has been previously reported from the reaction of UCl_4 with 4 equiv. of $\text{Li}(\text{ditox})$.³⁶ We found that **1** can also be synthesized through the reaction of UCl_4 with 4 equiv. of $\text{MgCl}(\text{ditox})(\text{THF})$ in a toluene suspension that, upon subsequent workup from pentane and drying, gives **1** as a pale purple solid in 63% yield (Scheme 1). The successful synthesis of **1** was confirmed through ^1H NMR

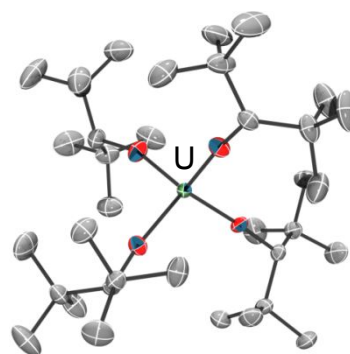


Figure 1. Solid-state molecular structure of **1**.

spectroscopy and its structure elucidated through single crystal X-ray diffractometry (Figure 1 and Table S1). The synthesis of **2** was accomplished following literature procedures.³⁸

Both **1** and **2** are highly soluble in non-polar solvents such as hexanes, and addition of excess degassed H_2O to these solutions under an inert atmosphere of N_2 results in the immediate precipitation of UO_2 as a dark solid upon stirring. Removal of the solvent under reduced pressure with mild heating (80°C) for several hours gives the UO_2 as a fine powder, which is subsequently thoroughly washed with THF and water in open air.

Nanoparticle characterization

The uranium dioxide powders synthesised from **1** ($\text{UO}_2\text{-1}$) and **2** ($\text{UO}_2\text{-2}$) were characterised by FT-IR and Raman spectroscopies and pXRD analysis. UO_2 possesses one broad absorption band in the IR region at 445 cm^{-1} but is otherwise featureless unless higher oxides are present.³⁹⁻⁴² As compared to the FT-IR (KBr pellet) of commercially purchased UO_2 , the spectra of $\text{UO}_2\text{-1}$ and $\text{UO}_2\text{-2}$ exhibit a few additional absorption bands, with a prominent peak in both at 906 cm^{-1} and a peak at 1550 cm^{-1} in $\text{UO}_2\text{-1}$, absorptions that cannot be attributed to hyperstoichiometric UO_{2+x} (Fig. S7).^{41, 42} Based upon the lack of additional features in the IR spectra, we tentatively assign these bands to the presence of residual organic material. In addition, there is a broad, ill-defined shoulder at ca. 750 cm^{-1} in $\text{UO}_2\text{-1}$, which has been shown to appear in samples of hyperstoichiometric UO_{2+x} ,⁴² signifying a higher oxide content.

The Raman spectra of $\text{UO}_2\text{-1}$ and $\text{UO}_2\text{-2}$ are qualitatively similar, with both samples giving weak signals (Fig. S8). Comparison of the Raman spectra of $\text{UO}_2\text{-1}$ and $\text{UO}_2\text{-2}$ with literature values show that

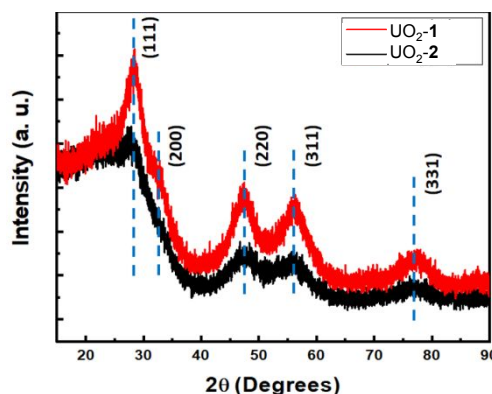


Figure 2. Comparison of the pXRD patterns obtained for the powders of $\text{UO}_2\text{-1}$ (red) and $\text{UO}_2\text{-2}$ (black).

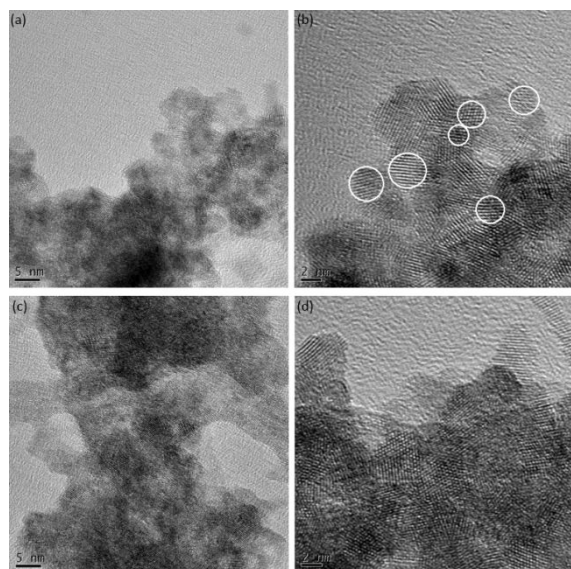


Figure 3. HRTEM images of the nanoparticles formed from UO₂-1 ((a)/(b)), and UO₂-2 ((c)/(d)) at different resolutions. White circles indicate location of discrete nanoparticles.

the spectra match most closely with hyperstoichiometric uranium dioxide of the formulation UO_{2+x} ($x = 0.12 - 0.20$),⁴³ consistent with the FT-IR data. However, caution is exercised here as determining the hyperstoichiometric oxygen content is not trivial and is further complicated by the fact that the presence or incorporation of U₄O₉ in UO₂-1 and UO₂-2 is not indiscernible by pXRD (vide supra).^{39, 44}

The pXRD patterns obtained for UO₂-1 and UO₂-2 are shown in Figure 2. Although several experimental procedures were attempted to optimize the resolution of the powder spectra, all efforts gave broad features with low peak resolution. This behaviour is consistent with a lack of crystallinity or, in accordance with the Scherrer equation, the presence of crystallites with small particle domain size indicating a nanocrystalline material.⁴⁵ Moreover, the counts for UO₂-1 are higher for each reflection under the same experimental conditions, suggesting greater crystallinity for the material prepared from **1**. UO₂-1 and UO₂-2 give reflections at (111), (200), (220), (311), and (331), matching the expected pattern for UO₂.^{39, 46} X-ray diffraction analysis can be used to determine the amount of incorporated oxygen in hyperstoichiometric UO_{2+x},^{39, 46} though, while the *hkl* reflections observed are consistent with uranium dioxide in the cubic fluorite form, the peak broadening and the poor signal to noise ratios preclude a definitive analysis of the uranium to oxygen ratio.

To better characterise the morphology of the UO₂ powders and to determine their crystalline properties, HRTEM analysis was performed. The bright field images of UO₂-1 and UO₂-2 are shown in Figure 3 and reveal that the powders produced from the hydrolysis of **1** and **2** are comprised of nanoparticles (NPs) approximately 3 nm in size. The size distribution of the NPs for both samples were calculated using ImageJ software.⁴⁷ The histograms of the size distributions are shown in Figure S9. However, the NPs are less coalesced with sharper lattices in the case of UO₂-1 as compared to UO₂-2. The discrete NPs of UO₂-1 are marked in Figure 3(b).

To further elucidate the crystallinity of the NPs, HRTEM fast Fourier transform (FFT) data was collected. The FFT images of UO₂-1 and UO₂-2 indicate the material to consist of polynanocrystalline

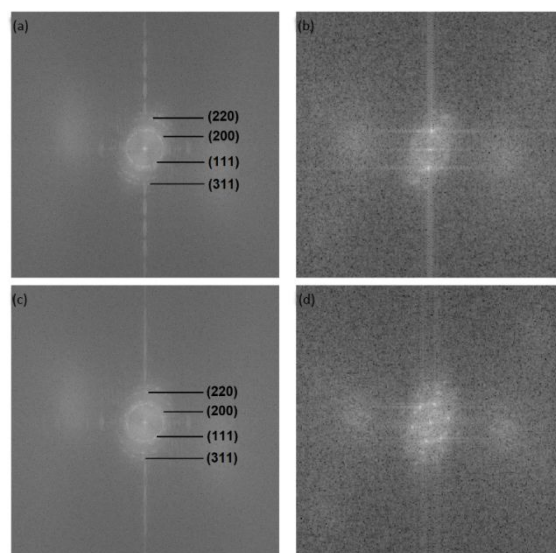


Figure 4. FFT images of UO₂-1 (a) and UO₂-2 (c) collected from the samples shown in Figure 4(b) and Figure 4(d), respectively, and the FFT patterns of selected areas in the UO₂-1 (b) and UO₂-2 (d) samples.

structures that give small spots that produce larger ring patterns (Fig. 4). The increased numbers of peaks in the FFT images of UO₂-2 (Figs. 4(c) and 4(d)), as compared to UO₂-1 (Figs. 4(a) and 4(b)), are consistent with increased aggregation of the nanoparticles, while the FFT pattern in Figure 4(b) is consistent with more discrete nanoparticles with some directionality.

The particles of UO₂-1 and UO₂-2 exist within the ultrasmall NP size regime (1-3 nm),⁴⁸ which is uncommon for uranium dioxide.^{28, 49-51} Of particular relevance to this point, Minasian and co-workers recently reported the synthesis of UO₂ NPs from the use of guest-host complexation of An(hfa)₄ (hfa = [(O)C(CF₃)₂CH₂]) within the carbon organic framework COF-5.⁵¹ The ultrasmall UO₂ NPs are formed within the COF-5 from thermal decomposition of the An(hfa)₄ in the presence of H₂O vapor, where the framework prevents aggregation to give particle sizes of 2-3 nm on average. Interestingly, while our synthetic procedure does not employ molecular templates, we are able to achieve a particle size comparable to their methods. We postulate this is due to hydrophobic conditions of the solution phase reaction which moderates the rate of hydrolysis; however, we cannot discount concentration effects, which is currently under study.

Thin film synthesis

In addition to their solubility in a wide range of organic solvents, **1** and **2** have the added advantage of being sublimable under relatively mild conditions (90 – 95 °C; 100 mTorr). This trait is desirable for the formation of thin films via CVD, making **1** and **2** appealing precursors for UO₂ thin film preparation. Moreover, this allows for the deposition of molecular films on various substrates with relative simplicity and without the use of specialized equipment. To demonstrate the viability of **1** and **2** as UO₂ thin film precursors, we set out to synthesize UO₂ films using readily available laboratory glassware.

Utilizing a two-piece sublimator, a glass or Si substrate (~1 cm × 1 cm) was taped to the cold finger and the apparatus was charged with 50 mg of **1** or **2**. The sublimator cold finger was

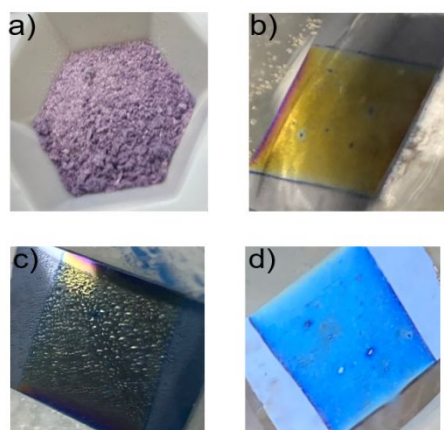


Figure 5. Images showing **1** (a) as a pure solid and its thin film deposition onto silicon (b), followed by condensation of water onto the film (c) resulting in the formation of $\text{UO}_2\text{-1}^{\text{film}}$ upon hydrolysis and drying (d).

cooled using a circulating, chilled water/ethylene glycol solution (5 °C) and the system subsequently placed under vacuum with heat. After approximately 1 h, visible film deposition was observed on the substrates and the heat was removed. The resulting films are stable at room temperature under inert atmospheres but are readily susceptible to hydrolysis. Utilizing Schlenk techniques, degassed water was introduced as a vapor under vacuum transfer. Upon exposure, a distinct colour change is observed for both **1** (Figure 5) and **2** (Figure S2). The resulting films were then heated on the substrates for 12 – 16 h at ~400 °C under dynamic vacuum.

Thin film characterisation

The formation of the UO_2 films using **1** ($\text{UO}_2\text{-1}^{\text{film}}$) were confirmed by pXRD analysis both on the glass and silicon substrates. As shown in Figure 6, the diffraction pattern obtained from the hydrolysis of **1** on silicon and glass compares favourably to commercially obtained UO_2 powder. On the other hand, no discernible peaks were observed in the pXRD analysis of the thin films produced from the hydrolysis of **2** (Fig. S2), thus the composition of the thin film material is not currently known. It is possible that this occurs due to incomplete hydrolysis of **2**, giving a mixture of products, or formation of a highly amorphous thin film.

Comparing the diffractions of $\text{UO}_2\text{-1}^{\text{film}}$ to the UO_2 standard, many of the expected hkl reflections are present on the thin films from 10 – 90° 2 θ , with peaks for the (111), (200), (220), (311), (222), and (331) indices all present. As with the pXRD of the powder samples, all of the 4th order diffractions are missing in the films. The absence of these peaks may be due to the poor signal to noise ratio for the samples, which may obscure their identification. Alternatively, the missing diffractions may indicate the morphological preference of the materials grown via our synthetic procedure. Previous reports of UO_2 film deposition have shown the propensity for preferred crystallographic orientation.^{35, 52, 53}

Further examination of the pXRD diffraction pattern reveals the presence of two additional peaks located at 21.2° and 43.5° 2 θ in $\text{UO}_2\text{-1}^{\text{film}}$ on the silicon substrate (Figure 6). We attribute

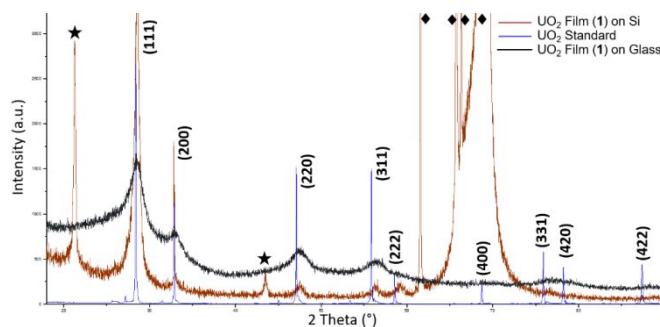


Figure 6. Comparison of pXRD patterns obtained for $\text{UO}_2\text{-1}^{\text{film}}$ silicon (red) and glass (black) as well as a UO_2 standard for reference (blue). ◆ indicate the diffractions due to the Si substrate. ★ indicate the presence of U_3O_8 .

these peaks to the formation of the mixed valent oxide species U_3O_8 . Specifically, these lattice spacings are consistent with the (001) and (220) hkl orientations. The formation of the U_3O_8 is unique to the silicon substrate as these peaks are absent in the $\text{UO}_2\text{-1}^{\text{film}}$ on glass and in the powders of $\text{UO}_2\text{-1}$. The reason for the partial oxidation of the UO_2 to U_3O_8 is not known at present and various preparations of the silicon substrate are currently under investigation.

Slight peak broadening is observed for the pXRD features of the thin films as compared to the UO_2 standard powder sample. Particle size calculation of the $\text{UO}_2\text{-1}^{\text{film}}$ on the silicon substrate, using the Scherrer equation, yields average particle size of 12.0 nm. This is significantly larger than those determined by HRTEM (~3 nm) in the powder samples of $\text{UO}_2\text{-1}$. The larger grain size may account for the overall improvement in the crystallinity, allowing for the appearance and identification of additional lattice indices as compared to $\text{UO}_2\text{-1}$ and $\text{UO}_2\text{-2}$.

The composition of $\text{UO}_2\text{-1}^{\text{film}}$ was additionally characterised by UV-visible (UV-vis) spectroscopy. A UV-vis spectrum was collected on $\text{UO}_2\text{-1}^{\text{film}}$ deposited on the transparent glass substrate. The spectrum shows a broad absorption feature with an onset around 665 nm but with a notable increase of absorption intensity near 400 nm (Fig. S5). The absorption trace is otherwise featureless, which is distinctive from stoichiometric UO_2 thin films that display broad but defined absorption peaks between ca. 250 – 500 nm.⁵⁴ Instead, the UV-vis spectrum of $\text{UO}_2\text{-1}^{\text{film}}$ on glass compares more favourably with that reported for $\text{UO}_{2.23}$,⁵⁴ indicating hyperstoichiometric oxygen content similar to that found for $\text{UO}_2\text{-1}$ and $\text{UO}_2\text{-2}$.

Finally, the thickness of the $\text{UO}_2\text{-1}^{\text{film}}$ produced on glass and silicon was determined using a stylus profiler. The sublimation and hydrolysis process as described produces thin films that range from approximately 15 – 40 nm (Figs. S3 and S4), demonstrating the viability of our method for the synthesis of UO_2 thin films in the nanometre regime. Current efforts are ongoing to study the surface characteristics and the electronic properties of these films and will be reported in due time.

Summary

We demonstrate that UO_2 NPs can be readily accessed from the hydrolysis of the molecular, tetravalent uranium precursors **1** and **2** to give $\text{UO}_2\text{-1}$ and $\text{UO}_2\text{-2}$, respectively. The NPs are formed from a modified sol-gel synthesis conducted under mild

conditions using standard laboratory equipment. The NPs produced in this fashion exist on the ultrasmall particle regime. Furthermore, **1** has added versatility as it can be sublimed with mild heating under vacuum to give thin films that are readily hydrolysed to $\text{UO}_2\text{-1}^{\text{film}}$, obviating the need for specialized CVD equipment. In all cases, the uranium dioxide formed is hyperstoichiometric in oxygen, giving UO_{2+x} . This may be due to surface oxidation of the NPs and thin films or as a result of oxygen diffusion based upon the surface morphology of the uranium dioxide materials.⁵⁵ Regardless, uranium oxides of the form UO_{2+x} are semiconductors, and our protocols add to the toolbox for the synthesis of these novel materials.

Experimental

General considerations

All air and moisture-sensitive operations were performed in a M. Braun dry box under an atmosphere of purified dinitrogen or using high vacuum standard Schlenk techniques. Solvents were dried using a Pure Process Technology Solvent Purification System and subsequently stored under a dinitrogen atmosphere over activated 4 Å molecular sieves. UCl_4 was synthesized using previously reported methods.⁵⁶ $\text{MgCl}(\text{ditox})(\text{THF})$ was synthesized using a modified procedure⁵⁷ from the reaction of $\text{MgCl}(\text{tBu})$ with hexamethylacetone in hexanes. $\text{U}(\text{CH}_2\text{SiMe}_2\text{NSiMe}_3)[\text{N}(\text{SiMe}_3)_2]_2$ (**2**) was synthesized as previously reported.³⁸ UO_2 powder was purchased from International Bio-Analytical Laboratories, Inc. and was used as received. Benzene- d_6 was purchased from Cambridge Isotope Laboratories Inc. and dried over activated 4 Å molecular sieves for 24 h prior to use. Celite used for filtration was dried under vacuum while heating at 250 °C for 24 h, subsequently cooled under vacuum, and stored under dinitrogen. NMR spectra were recorded using a Bruker AVANCE II 400 MHz spectrometer. ^1H NMR spectra are referenced to SiMe_4 using the residual ^1H solvent peaks as internal standard. UV-vis-NIR spectra were recorded using a Cary 5000 spectrophotometer in toluene, or as films using the Cary solid state sample holder in transmission geometry. Fourier transform infrared (FT-IR) spectra were recorded on a Bruker Tensor 27 infrared spectrometer (ATR) from powder samples. Profilometry was conducted using a KLA stylus type Tencor profilometer. Raman spectra of the $\text{UO}_2\text{-1}$ and $\text{UO}_2\text{-2}$ powder samples were measured with an NTEGRA Spectra-II (NT-MDT) Raman spectrometer equipped with a 532 nm laser excitation source with an 100x objective.

X-ray diffraction details

Data for **1** was collected on a dual-source Bruker Venture D8 4-axis diffractometer equipped with a PHOTON II CPAD detector with a $1\mu\text{S}$ Mo $\text{K}\alpha$ X-ray source ($\alpha = 0.71073$ Å) fitted with a HELIOS MX monochromator. The crystals were mounted on a Mitigen Kapton loop coated in NVH oil and maintained at 100(2) K under a flow of nitrogen gas during data collection. Data collection and cell parameter determination were conducted using the SMART⁵⁸ program. Integration of the data and final cell parameter refinements were performed using SAINT⁵⁹ software with data absorption correction implemented through SADABS.⁶⁰ Structures were solved using intrinsic phasing methods and difference Fourier

techniques. All hydrogen atom positions were idealized and rode on the atom of attachment. Structure solution, refinement, graphics, and creation of publication materials were performed using SHELXTL⁶¹ or the Olex2⁶² crystallographic package. Crystallographic parameters for **1** are shown in Table S1. CCDC deposit number 2106529 for **1**.

Powder X-ray diffraction was carried out either on a θ - θ configuration on a Rigaku Smart Lab double-axis diffractometer using Cu- $\text{K}\alpha$ radiation (1.540 Å) radiation or a Panalytical Empyrean 2 instrument equipped with a flat sample stage with 45 kV and 40 mA with Cu- $\text{K}\alpha$ radiation ($\lambda = 1.540$ Å). Commercially available UO_2 powder reference was measured on a spinning sample stage at 2 RPS on a low background Si sample holder. All X-ray data was processed using PANalytical HighScore (Plus) software package.

High resolution transmission electron microscopy (HRTEM)

HRTEM was performed with a 200 kV JEOL JEM 2100F system. A small amount of powder (< 0.5 mg) was randomly sampled and dispersed by ethanol in a microcentrifuge tube followed by ultrasonic deagglomeration to separate the soft agglomerates into individual grains. The suspension was then pipetted onto a copper grid, and the ethanol was left under an infrared heater to evaporate. The fast Fourier transform (FFT) method was applied to convert the crystalline contribution in a real space image into lattice reflections of a reciprocal space image.

Synthesis of $\text{U}(\text{ditox})_4$ (**1**)

Synthesis of **1** was carried out via a modified synthetic procedure based upon a previously described synthesis.³⁷ In a 100 mL round bottom flask, 0.5 g (1.82 mmol) of $\text{MgCl}(\text{ditox})(\text{THF})$ was added to a stirring toluene (20 mL) suspension containing 0.16 g (0.41 mmol) of UCl_4 . The dark green suspension was stirred vigorously at room temperature for 72 h. The resulting turbid, light blue-green suspension was dried completely under vacuum to a blue solid. The solid was dissolved in diethyl ether (50 mL) and stirred at room temperature for 1 h, producing a light violet turbid suspension. This suspension was filtered through Celite supported on a medium porosity glass frit, giving a purple filtrate. The Celite was subsequently washed with diethyl ether (5 mL \times 2). The filtrate was concentrated to approximately 2 mL and the solution stored at -35 °C. After 48 h, violet crystals appear which could be isolated after removal of the supernatant and drying under vacuum. Yield: 0.21 g, 63%. ^1H NMR (25 °C, 400 MHz, C_6D_6): δ 0.14 (s, 72H, Me_3CH), δ 31.85 (s, 4H, Me_3CH). UV-vis (toluene, 1.60 mM, 25 °C, $\text{L}\cdot\text{mol}^{-1}\cdot\text{cm}^{-1}$): 284 ($\epsilon = 1535$), 459 ($\epsilon = 8$), 515 ($\epsilon = 19$), 572 ($\epsilon = 14$), 667 ($\epsilon = 58$), 701 ($\epsilon = 19$), 779 ($\epsilon = 10$), 919 ($\epsilon = 6$), 1039 ($\epsilon = 12$), 1173 ($\epsilon = 24$), 1316 ($\epsilon = 19$), 1404 ($\epsilon = 10$). The ^1H NMR spectrum of **1** (Fig. S1) matches the reported values.³⁷

Synthesis of $\text{UO}_2\text{-1}$ and $\text{UO}_2\text{-2}$ via room temperature hydrolysis of **1** and **2**

Hydrolysis of both **1** and **2** were performed in the following manner: In a glovebox, **1** or **2** (0.5 g) were loaded into a Cajon flask (50 mL) and hexanes or pentane (5 mL) was added to dissolve the solid, giving a violet solution. The Cajon flask was sealed, removed from the

glovebox, and subsequently attached to a Schlenk line. Under a purge of dinitrogen, 1.0 mL of degassed, reverse osmosis treated water was added to the uranium solution. Immediate formation of a black-tan precipitate was observed. The Cajon flask was then sealed and the resulting dark suspension stirred for 10 – 15 min at room temperature. The solvent was then removed in vacuo, leaving a dark, almost black solid, which was dried for 12 h at 80 °C. The grey-black solid was then washed with THF (50 mL) in air. The dark solid was collected by vacuum filtration on a small medium porosity glass frit. The dark powder was washed on the frit with deionized water (10 mL) and dried for 1-2 h under vacuum with mild heating (80 °C) to give UO₂-1 or UO₂-2 in 84 and 89% yield, respectively.

Conflicts of interest

There are no conflicts to declare.

Acknowledgements

We are grateful to the NSF (DMR-1827745; CHE-1827875) and the Welch Foundation (AH-1922-20200401; S.F.) for financial support of this work. S.F. is an Alfred P. Sloan Foundation research fellow and is thankful for their support. D.P. and S.C. wish to express sincere thanks to the Sophisticated Analytical Instrument Facility (SAIF), Indian Institute of Technology (IIT) - Bombay for the HRTEM, and central HRXRD facility in the Department of Physics, IIT Bombay, India.

Notes and references

- S. H. Taylor, in *Metal Oxide Catalysis*, eds. S. D. Jackson and J. S. J. Hargreaves, Wiley-VCH Verlag GmbH & Co., 2008, DOI: <https://doi.org/10.1002/9783527626113.ch13>, pp. 539-560.
- S. V. Chong, M. A. Barteau and H. Idriss, The influence of surface defects on ethanol dehydrogenation versus dehydration on the UO₂(111) surface, *Catal. Today*, 2000, **63**, 283-289.
- Z. R. Ismagilov and S. V. Lazareva, Synthesis and Characterization of Uranium-containing Catalysts, *Catal. Rev.*, 2013, **55**, 135-209.
- Q. Wang, G.-D. Li, S. Xu, J.-X. Li and J.-S. Chen, Synthesis of uranium oxide nanoparticles and their catalytic performance for benzyl alcohol conversion to benzaldehyde, *J. Mater. Chem.*, 2008, **18**, 1146-1152.
- K. Shrestha, T. Yao, J. Lian, D. Antonio, M. Sessim, M. R. Tonks and K. Gofryk, The grain-size effect on thermal conductivity of uranium dioxide, *J. Appl. Phys.*, 2019, **126**.
- Y. Q. An, A. J. Taylor, S. D. Conradson, S. A. Trugman, T. Durakiewicz and G. Rodriguez, Ultrafast Hopping Dynamics of 5f Electrons in the Mott Insulator UO₂ Studied by Femtosecond Pump-Probe Spectroscopy, *Phys. Rev. Lett.*, 2011, **106**, 207402.
- L. E. Roy, T. Durakiewicz, R. L. Martin, J. E. Peralta, G. E. Scuseria, C. G. Olson, J. J. Joyce and E. Guziewicz, Dispersion in the Mott insulator UO₂: A comparison of photoemission spectroscopy and screened hybrid density functional theory, *J. Comput. Chem.*, 2008, **29**, 2288-2294.
- J. Schoenes, Optical-Properties and Electronic-Structure of UO₂, *J. Appl. Phys.*, 1978, **49**, 1463-1465.
- H. M. He, D. A. Andersson, D. D. Allred and K. D. Rector, Determination of the Insulation Gap of Uranium Oxides by Spectroscopic Ellipsometry and Density Functional Theory, *J. Phys. Chem. C*, 2013, **117**, 16540-16551.
- H. L. Shi, M. F. Chu and P. Zhang, Optical properties of UO₂ and PuO₂, *J. Nucl. Mater.*, 2010, **400**, 151-156.
- F. N. Skomurski, J. W. Wang, R. C. Ewing and U. Becker, Charge distribution and oxygen diffusion in hyperstoichiometric uranium dioxide UO_{2+x} (x ≤ 0.25), *J. Nucl. Mater.*, 2013, **434**, 422-433.
- T. P. Kaloni, N. Onder, J. Pencer and E. Torres, DFT+U approach on the electronic and thermal properties of hypostoichiometric UO₂, *Ann. Nucl. Chem.*, 2020, **144**, 107511.
- T. T. Meek and B. von Roedern, Semiconductor devices fabricated from actinide oxides, *Vacuum*, 2008, **83**, 226-228.
- L. Ding, J. Leduc, T. Fischer, S. Mathur and Y. Li, Gelation of uranyl ions and gel-derived uranium oxide nanoparticles for gas sensing, *Nanoscale Adv.*, 2020, **2**, 2478-2484.
- J. L. Bates, C. A. Hinman and T. Kawada, Electrical Conductivity of Uranium Dioxide, *J. Am. Ceram. Soc.*, 1967, **50**, 652-&.
- P. Ruello, G. Petot-Ervas and C. Petot, Electrical conductivity and thermoelectric power of uranium dioxide, *J. Am. Ceram. Soc.*, 2005, **88**, 604-611.
- H. Hausner, Determination of the melting point of uranium dioxide, *J. Nucl. Mater.*, 1965, **15**, 179-183.
- J. L. Lin, I. Dahan, B. Valderrama and M. V. Manuel, Structure and properties of uranium oxide thin films deposited by pulsed dc magnetron sputtering, *Appl. Surf. Sci.*, 2014, **301**, 475-480.
- P. Kovacheva, G. Avdeev and D. Todorovsky, Mechanochemically induced synthesis of UO_{2+x} and uranium-thorium mixed oxides from sol-gel produced precursors, *J. Radioanal. Nucl. Chem.*, 2011, **287**, 519-524.
- E. Zimmer, C. Ganguly, J. Borchardt and H. Langen, Sgmp - an Advanced Method for Fabrication of UO₂ and Mox Fuel Pellets, *J. Nucl. Mater.*, 1988, **152**, 169-177.
- V. N. Vaidya, S. K. Mukerjee, J. K. Joshi, R. V. Kamat and D. D. Sood, A Study of Chemical-Parameters of the Internal Gelation Based Sol-Gel Process for Uranium-Dioxide, *J. Nucl. Mater.*, 1987, **148**, 324-331.
- Y. J. Cheng, X. Y. Xu, S. G. Yan, X. H. Pan, Z. Chen and Z. Lin, Hydrothermal growth of large-size UO₂ nanoparticles mediated by biomass and environmental implications, *RSC Adv.*, 2014, **4**, 62476-62482.
- O. Walter, K. Popa and O. D. Blanco, Hydrothermal decomposition of actinide(IV) oxalates: a new aqueous route towards reactive actinide oxide nanocrystals, *Open Chem.*, 2016, **14**, 170-174.
- J. Manaud, J. Maynadié, A. Mesbah, M. O. J. Y. Hunault, P. M. Martin, M. Zunino, D. Meyer, N. Dacheux and N. Clavier, Hydrothermal Conversion of Uranium(IV) Oxalate into Oxides: A Comprehensive Study, *Inorg. Chem.*, 2020, **59**, 3260-3273.
- K. Popa, O. Walter, O. D. Blanco, A. Guiot, D. Bouëxière, J.-Y. Colle, L. Martel, M. Naji and D. Manara, A low-temperature synthesis method for AnO₂ nanocrystals (An

- = Th, U, Np, and Pu) and associate solid solutions, *CrystEngComm*, 2018, **20**, 4614-4622.
26. L. Balice, D. Bouëxière, M. Cologna, A. Cambriani, J.-F. Vigier, E. De Bona, G. D. Soraru, C. Kübel, O. Walter and K. Popa, Nano and micro $U_{1-x}Th_xO_2$ solid solutions: From powders to pellets, *J. Nucl. Mater.*, 2018, **498**, 307-313.
27. V. Trillaud, J. Maynadié, J. Manaud, J. Hidalgo, D. Meyer, R. Podor, N. Dacheux and N. Clavier, Synthesis of size-controlled UO_2 microspheres from the hydrothermal conversion of U(IV) aspartate, *CrystEngComm*, 2018, **20**, 7749-7760.
28. T. M. Nenoff, B. W. Jacobs, D. B. Robinson, P. P. Provencio, J. Huang, S. Ferreira and D. J. Hanson, Synthesis and Low Temperature In Situ Sintering of Uranium Oxide Nanoparticles, *Chem. Mater.*, 2011, **23**, 5185-5190.
29. M. C. Rath, D. B. Naik and S. K. Sarkar, Reversible growth of UO_2 nanoparticles in aqueous solutions through 7 MeV electron beam irradiation, *J. Nucl. Mater.*, 2013, **438**, 26-31.
30. Y.-M. Wang, Q.-D. Chen and X.-H. Shen, One-step synthesis of hollow UO_2 nanospheres via radiolytic reduction of ammonium uranyl tricarbonate, *Chin. Chem. Lett.*, 2017, **28**, 197-200.
31. E. Gerber, A. Y. Romanchuk, S. Weiss, S. Bauters, B. Schacherl, T. Vitova, R. Hubner, S. S. A. Azzam, D. Detollenaere, D. Banerjee, S. M. Butorin, S. N. Kalmykov and K. O. Kvashnina, Insight into the structure-property relationship of UO_2 nanoparticles, *Inorg. Chem. Front.*, 2021, **8**, 1102-1110.
32. R. Jovani-Abril, M. Gibilaro, A. Janßen, R. Eloirdi, J. Somers, J. Spino and R. Malmbeck, Synthesis of nc- UO_2 by controlled precipitation in aqueous phase, *J. Nucl. Mater.*, 2016, **477**, 298-304.
33. L. Appel, J. Leduc, C. L. Webster, J. W. Ziller, W. J. Evans and S. Mathur, Synthesis of Air-Stable, Volatile Uranium(IV) and (VI) Compounds and Their Gas-Phase Conversion To Uranium Oxide Films, *Angew. Chem. Int. Ed.*, 2015, **54**, 2209-2213.
34. M. D. Straub, J. Leduc, M. Frank, A. Raauf, T. D. Lohrey, S. G. Minasian, S. Mathur and J. Arnold, Chemical Vapor Deposition of Phase-Pure Uranium Dioxide Thin Films from Uranium(IV) Amidate Precursors, *Angew. Chem. Int. Ed.*, 2019, **58**, 5749-5753.
35. A. Raauf, J. Leduc, M. Frank, D. Stadler, D. Graf, M. Wilhelm, M. Grosch and S. Mathur, Magnetic Field-Assisted Chemical Vapor Deposition of UO_2 Thin Films, *Inorg. Chem.*, 2021, **60**, 1915-1921.
36. J. L. Stewart and R. A. Andersen, Preparation and Crystal-Structure of the Addition Compound $MeLi.U[OCH(CMe_3)_2]_4$, a Compound with a Uranium to Carbon Sigma-Bond, *J. Chem. Soc., Chem. Commun.*, 1987, 1846-1847.
37. J. L. Stewart, *Tris(bis(trimethylsilyl)amido)uranium: Compounds with tri-, tetra-, and penta-valent uranium*, Report LBL-25240; Other: ON: DE88010356 United States 10.2172/5100151 Other: ON: DE88010356 NTIS, PC A10/MF A01; 3. LBNL English, ; Lawrence Berkeley Lab., CA (USA), 1988.
38. S. J. Simpson, H. W. Turner and R. A. Andersen, Preparation and hydrogen-deuterium exchange of alkyl and hydride bis(trimethylsilyl)amido derivatives of the actinide elements, *Inorg. Chem.*, 1981, **20**, 2991-2995.
39. J. M. Elorrieta, L. J. Bonales, N. Rodriguez-Villagra, V. G. Baonza and J. Cobos, A detailed Raman and X-ray study of UO_{2+x} oxides and related structure transitions, *Phys. Chem. Chem. Phys.*, 2016, **18**, 28209-28216.
40. G. Lu, A. J. Haes and T. Z. Forbes, Detection and identification of solids, surfaces, and solutions of uranium using vibrational spectroscopy, *Coord. Chem. Rev.*, 2018, **374**, 314-344.
41. G. C. Allen, J. A. Crofts and A. J. Griffiths, Infrared spectroscopy of the uranium/oxygen system, *J. Nucl. Mater.*, 1976, **62**, 273-281.
42. J. G. Kim, Y. S. Park, Y. K. Ha and K. Song, Infrared Spectra of Uranium Oxides Measured by ATR-FTIR, *J. Nucl. Sci. Tech.*, 2009, **46**, 1188-1192.
43. D. Manara and B. Renker, Raman spectra of stoichiometric and hyperstoichiometric uranium dioxide, *J. Nucl. Mater.*, 2003, **321**, 233-237.
44. L. Desgranges, G. Baldinozzi, P. Simon, G. Guimbretiere and A. Canizares, Raman spectrum of U_4O_9 : a new interpretation of damage lines in UO_2 , *J. Raman Spectrosc.*, 2012, **43**, 455-458.
45. C. F. Holder and R. E. Schaak, Tutorial on Powder X-ray Diffraction for Characterizing Nanoscale Materials, *ACS Nano*, 2019, **13**, 7359-7365.
46. H. M. He and D. Shoesmith, Raman spectroscopic studies of defect structures and phase transition in hyperstoichiometric UO_{2+x} , *Phys. Chem. Chem. Phys.*, 2010, **12**, 8108-8117.
47. C. A. Schneider, W. S. Rasband and K. W. Eliceiri, NIH Image to ImageJ: 25 years of image analysis, *Nat. Methods.*, 2012, **9**, 671-675.
48. B. H. Kim, M. J. Hackett, J. Park and T. Hyeon, Synthesis, Characterization, and Application of Ultrasmall Nanoparticles, *Chem. Mater.*, 2014, **26**, 59-71.
49. E. J. O'Loughlin, S. D. Kelly, R. E. Cook, R. Csencsits and K. M. Kemner, Reduction of Uranium(VI) by mixed iron(II/iron(III) hydroxide (green rust): Formation of UO_2 nanoparticles, *Environ. Sci. Technol.*, 2003, **37**, 721-727.
50. D. Hudry, C. Apostolidis, O. Walter, T. Gouder, E. Courtois, C. Kübel and D. Meyer, Controlled Synthesis of Thorium and Uranium Oxide Nanocrystals, *Chem. Eur. J.*, 2013, **19**, 5297-5305.
51. L. M. Moreau, A. Herve, M. D. Straub, D. R. Russo, R. J. Abergel, S. Alayoglu, J. Arnold, A. Braun, G. J. P. Deblonde, Y. Liu, T. D. Lohrey, D. T. Olive, Y. Qiao, J. A. Rees, D. K. Shuh, S. J. Teat, C. H. Booth and S. G. Minasian, Structural properties of ultra-small thorium and uranium dioxide nanoparticles embedded in a covalent organic framework, *Chem. Sci.*, 2020, **11**, 4648-4668.
52. Y. A. Teterin, A. J. Popel, K. I. Maslakov, A. Y. Teterin, K. E. Ivanov, S. N. Kalmykov, R. Springell, T. B. Scott and I. Farnan, XPS Study of Ion Irradiated and Unirradiated UO_2 Thin Films, *Inorg. Chem.*, 2016, **55**, 8059-8070.
53. J. Lin, I. Dahan, B. Valderrama and M. V. Manuel, Structure and properties of uranium oxide thin films deposited by pulsed dc magnetron sputtering, *Appl. Surf. Sci.*, 2014, **301**, 475-480.
54. R. J. Ackermann, R. J. Thorn and G. H. Winslow, Visible and Ultraviolet Absorption Properties of Uranium Dioxide Films, *J. Opt. Soc. Am.*, 1959, **49**, 1107-1111.
55. B. Dorado, P. Garcia, G. Carlot, C. Davoisne, M. Fraczkiewicz, B. Pasquet, M. Freyss, C. Valot, G. Baldinozzi,

- D. Siméone and M. Bertolus, First-principles calculation and experimental study of oxygen diffusion in uranium dioxide, *Phys. Rev. B*, 2011, **83**, 035126.
56. J. L. Kiplinger, D. E. Morris, B. L. Scott and C. J. Burns, Convenient Synthesis, Structure, and Reactivity of $(C_5Me_5)U(CH_2C_6H_5)_3$: A Simple Strategy for the Preparation of Monopentamethylcyclopentadienyl Uranium(IV) Complexes, *Organometallics*, 2002, **21**, 5978-5982.
57. G. A. Olah, A. H. Wu, O. Farooq and G. K. S. Prakash, Synthetic methods and reactions. 146. Olefins from crowded carbonyl compounds with tert-butyllithium (tert-butylmagnesium chloride)/thionyl chloride. Study of carbocationic reaction intermediates and rearrangement-cleavage under stable ion conditions using carbon-13 NMR spectroscopy, *J. Org. Chem.*, 1990, **55**, 1792-1796.
58. SMART Apex II, Version 2.1; Bruker AXS Inc.: Madison, WI
59. SAINT Software User's Guide, Version 7.34a; Bruker AXS Inc.: Madison, WI
60. Blessing, R. *Acta Crystallogr. A* 1995, **A51**
61. Sheldrick, G. M. SHELXTL, 6.12; Bruker Analytical X-Ray Systems, Inc.: Madison, WI
62. Dolomanov, O. V.; Bourhis, L. J.; Gildea, R. J.; Howard, J. A. K.; Puschmann, H. J. *Appl. Cryst.* 2009, **42**, 339